Available online at www.sciencedirect.com

ScienceDirect

Energy Procedia 8 (2011) 337–342

Energy Procedia

SiliconPV: 17-20 April 2011, Freiburg, Germany

Recombination at local aluminum-alloyed silicon solar cell base contacts by dynamic infrared lifetime mapping

Jens Müller[a], Karsten Bothe[a], Sebastian Gatz[a], Heiko Plagwitz[b], Gunnar Schubert[b], Rolf Brendel[a,c]

[a] *Institute for Solar Energy Research Hamelin (ISFH), Am Ohrberg 1, 31860 Emmerthal, Germany*
[b] *Sunways AG, Macairestraße 3 - 5,78467 Konstanz, Germany*
[c] *Institute for Solid State Physics, Leibniz Universität Hannover, Appelstrasse 2, 30167 Hannover, Germany*

Abstract

The application of local aluminum (Al)-alloyed contacts to the *p*-type base of silicon solar cells reduces minority charge carrier recombination due to the formation of a local back surface field (LBSF). We study the recombination properties and formation of base contacts, which are realized by local laser ablation of a dielectric stack (laser contact opening - LCO) and subsequent full area screen printing of Al paste. Based on charge carrier lifetime measurements using the camera-based and calibration-free dynamic infrared lifetime mapping (ILM) technique, we determine contact recombination velocities at the contacts as low as S_{cont} = 65 cm/s on 200 Ωcm float-zone silicon (FZ-Si) and corresponding reverse saturation current densities of $J_{0,cont}$ = 900 fA/cm² on 1.5 Ωcm FZ-Si. As a result we show that local contact geometries with point contact radii r > 100 µm and line contact widths a > 80 µm are appropriate for lowest contact recombination employing local Al alloyed contacts. Furthermore, complete and high quality laser ablation of the dielectric stack is necessary for the formation of a sufficiently thick LBSF.

Selection and/or peer-review under responsibility of SiliconPV 2011

local back surface field; carrier lifetime; laser ablation; silicon solar cells

1. Introduction

Full area screen printing and firing of Al paste is today's standard rear side contacting technique for crystalline Si solar cells. The back surface field (BSF) generated by a highly Al-doped layer significantly reduces minority charge carrier recombination at the base contact. The application of Al-alloyed contacts to passivated emitter and rear cell (PERC) [1] structures is currently under investigation [2, 3]. These cells

1876–6102 © 2011 Published by Elsevier Ltd. Selection and/or peer-review under responsibility of SiliconPV 2011.
Open access under CC BY-NC-ND license. doi:10.1016/j.egypro.2011.06.146

comprise rear contacts through a locally opened dielectric layer. Effective rear surface recombination velocities down to 70 cm/s [2] on all screen-printed PERC-type silicon solar cells with efficiencies of up to 20.3 % [3] demonstrated the potential of local Al alloyed contacts.

Recent publications indicated that the contact formation is considerably affected by the processing conditions. Additives to the Al paste were shown to enhance the thickness and the uniformity of the LBSF [4]. Rear side metallization by stacks of Al and other metals significantly changed the local contact morphology [5]. Furthermore, a strong impact of the contact size on the dissolution of silicon during the alloying process and thus on the contact structure was expected [6].

The aim of this work is to quantify the recombination at local Al-alloyed contacts and to analyze the contact formation process with respect to processing parameters, i.e. contact geometry and laser used for the LCOs. We extract the contact recombination velocities S_{cont} as well as the contact's reverse saturation current densities $J_{0,cont}$ of local Al-alloyed base contacts from of area-averaged carrier lifetime measurements. For this we apply the approach introduced in Ref. 7. Lifetime data measured by the calibration-free dynamic infrared lifetime mapping (dyn-ILM) technique [8] is analyzed by an analytical model for the three dimensional charge carrier transport [9].

2. Sample preparation

The samples are (100)-oriented floatzone (FZ) *p*-type silicon 5" pseudo-square wafers of 1.5 and 230 Ωcm resistivity, with a thickness of 275 µm after saw-damage etching in KOH. After RCA cleaning followed by a HF dip, both surfaces are electronically passivated by a stack of approximately 17 nm thermal oxide (SiO_2) and 75 nm silicon nitride (SiN_x). The latter has a refractive index of n = 2.05. The oxide grows in dry O_2 ambient at 900°C. Using a parallel plate reactor, we deposit the SiN_x layers by plasma enhanced chemical vapor deposition at 400°C on both surfaces.

Single-sided laser contact openings (LCOs) are obtained by local laser ablation of the dielectric stack. We compare three different ablation processes at two laser wavelengths: i) 532nm, 10 ps long pulse length with a Gaussian beam profile (ps Laser) [10], ii) 355nm, 20 ns long pulse length with Gaussian beam profile (ns Laser 1) and iii) 532nm, 10 ns long pulse length with a flat-top beam profile (ns Laser 2) [11]. As shown in Fig. 1, we apply two different contacting geometries: a) parallel line contacts and b) equally spaced point contacts. We realize openings of radius *r* and line contacts of line width *a*, by overlapping single openings of 25 µm radius using the ps laser, 15 µm radius in the case of ns Laser 1 and 85 µm radius for ns Laser 2. The laser defines 16 contact geometries on the samples, each 2.5 × 2.5 cm^2 large. The geometries vary in contact pitch *p* or contact size (i.e. radius *r* or line width *a*). We complete the contact formation by full-area screen printing of a fritless Al paste on top of the LCOs and by firing the samples in an industrial conveyor belt furnace at an approximate wafer temperature of 800°C.

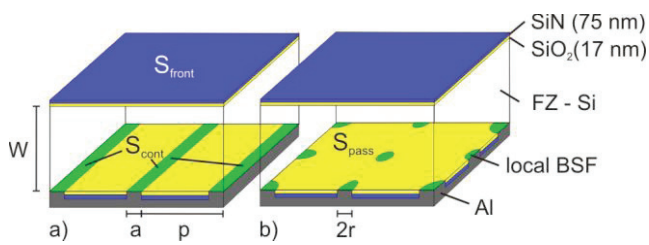

Figure 1. Schematics of the sample structures under test (not to scale). A dielectric stack consisting of 17 nm SiO_2 and 75 nm SiN on top is applied on both sides of FZ-Si wafers of 1.5 and 200 Ωcm resistivity. Laser contact openings (LCOs) are realized by laser ablation of the rear dielectric stack in a) line and b) point geometries. The contact formation is subsequently realized, by full-area screen printing and firing of a standard fritless Al paste.

3. Determination of contact recombination

To determine the local contact recombination, we follow the approach presented in Ref. 7. Dynamically calibrated steady state ILM [8] measures the effective charge carrier lifetime τ_{eff} under an illuminating photon flux of 3×10^{16} cm^{-2}s^{-1}. From this we determine the effective surface recombination velocities at the front S_{front} and rear S_{rear} of the samples that would yield the same effective lifetimes in a one-dimensional transport problem. The reverse saturation current density

$$J_{0,S} = e\frac{n_i^2}{N_A}S \tag{1}$$

is related to the recombination at one surface. It depends on the elementary charge e, the intrinsic charge carrier concentration $n_i \sim 10^{10}$ cm^{-3} at room temperature and the doping concentration N_A.

We apply Fischer's analytical model [9] to describe the area averaged effective rear surface recombination velocity

$$S_{eff,rear} = \left(\frac{R_s - \rho W}{\rho D} + \frac{1}{fS_{cont}}\right)^{-1} + \frac{S_{pass}}{1-f}, \tag{2}$$

that is a function of the base series resistance R_s, the base resistivity ρ, the sample thickness W, the diffusion coefficient D, the metallization area fraction f, and the surface recombination velocity in the passivated area S_{pass} as well as under the contact S_{cont}. The base series resistance R_s depends on the contact layout [12]. The contact pitches p as well as the point radii r and line widths a and thus the metallization fraction f of point $f_{\text{point}} = \pi r^2 / p^2$ and line contacts $f_{\text{point}} = a / p$ are determined with a light microscope prior to screen printing of the Al paste.

4. Results

Figure 2 a) and b) show $S_{\text{eff,rear}}$ on 200 Ωcm material processed with the ps Laser as a function of the metallization fraction f for line and point contacts, respectively. We shape large point and line contacts by a matrix of overlapping single point contacts. We calculate the radius r of non-circular shaped point contacts using their contact area $A = \pi r^2$. The metallization fraction f is calculated from the size of the

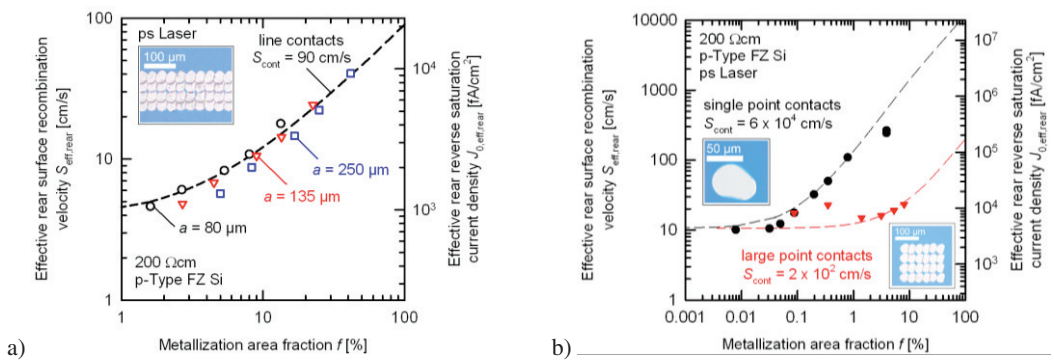

Figure 2. Effective rear surface recombination velocity $S_{\text{eff,rear}}$ and effective rear reverse saturation current density $J_{0,\text{eff,rear}}$ as a function of the metallization fraction f, measured at the samples in Fig. 2: a) line contacts of different line width a b) single point contacts of different pitch p (black circles) and large point contacts of different radius r (red triangles). The lines show the fit of the analytical model to the measured data. Line contacts and large point contacts are realized by overlapping of single point contacts, which is depicted in the small micrographs.

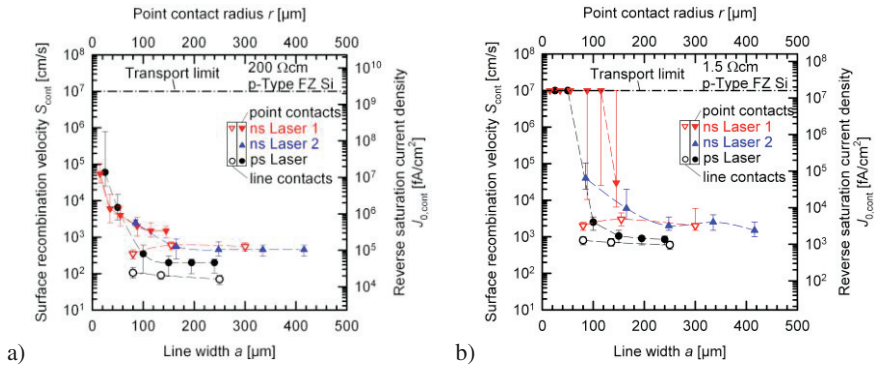

Figure 3. Contact recombination velocity S_{cont} and contact reverse saturation current density $J_{0,cont}$ at point contacts (closed symbols) as a function of the contact radius and line contacts (open symbols) as a function of the line width, measured on wafers of a) 200 Ωcm and b) 1.5 Ωcm resistivity. The lines are guides to the eye. The thermal velocity equals the transport limit.

LCOs as measured with a light microscope prior to screen printing of the Al paste. Employing the analytical model of Ref. 9 and a least squares fit with Eqn. 2 to the experimental data in Fig. 2, we obtain the contact recombination velocity S_{cont}. Note, that the contact size slightly increases during firing of the samples. Thus, all S_{cont} have to be regarded as upper limits for the actual values.

We find a low value of S_{cont} = 90 cm/s for line contacts when fitting the data in Fig. 2a, nearly independent of the line width. In comparison, the evaluation reveals $S_{cont} = 6 \times 10^4$ cm/s for single point contacts when fitting the data in Fig. 2b. However, the analysis of the large point contacts in Fig. 2b with a larger contact size does not result in the same large S_{cont} value as for single point contacts. Large point contacts are applied with constant pitch p = 1.5 mm, but differ in contact size. At the largest point contact with r = 240 µm we measure $S_{cont} = 2 \times 10^2$ cm/s, which is two orders of magnitude smaller, compared to S_{cont} of single point contacts with a radius of only 25 µm. Hence, the local recombination properties at the contacts change with contact size and geometry.

The contact recombination strongly depends on the LBSF thickness [13]. A thick Al-doped layer leads to low contact recombination velocities. Hence, the change of contact recombination with contact size and geometry in Fig. 2a) and b) is due to different LBSF thickness values. An analytical model in reference 13 describes the thickness of the LBSF as a function of the local contact formation using the phase diagram of Al and Si. The LBSF thickness strongly depends on the ratio m_{Al}/A, where m_{Al} is the mass of Al contributing to the melt of Si and Al and A is the interface area between Si and Al. A decrease in m_{Al}/A and thus reduced contact recombination can be achieved by using point or line contacts with a large interface area $A_{line} = a\ p$ in the case of line contacts and $A_{points} = \pi\ r^2$ for point contacts, which is in accordance to Fig. 2a) and b).

We analyze the local contact formation as a function of the sample resistivity and the laser used for the LCOs in Fig. 3. The same approach as used for the data in Fig. 2 is also applied to samples of a) 200 Ωcm and b) 1.5 Ωcm material. The thermal velocity of minority charge carriers is $v_{th} \sim 10^7$ cm/s and constitutes an upper limit for the surface recombination S_{cont} even in the case of an infinite surface recombination velocity. Our analysis assumes a measurement error of 20 % for all $S_{eff,rear}$ values which accounts for 10 % of systematic error and 10 % of statistical error.

In Fig. 3a) and b) the point contact data exhibit a decrease in S_{cont} with increasing contact size, independent of the material resistivity and the laser used. In contrast, the S_{cont} values of the line contacts are smaller and nearly independent of the line width a in the range $80 < a < 300$ µm in Fig. 3a) and b).

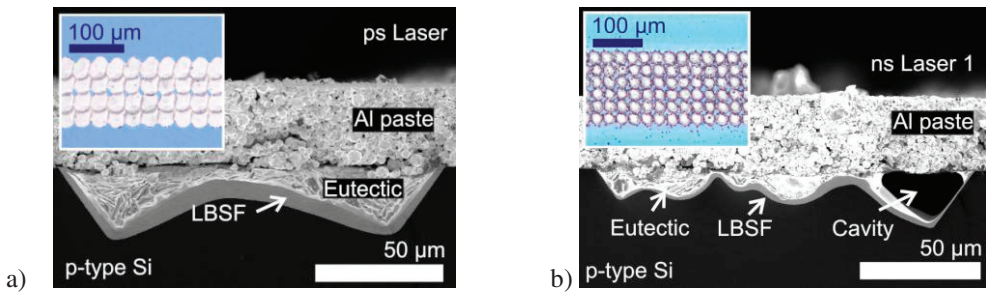

Fig . 4. SEM image of a) a ps Laser and b) ns Laser 1 line contact of a = 150 µm line width. In the upper left, a micrograph of the contacts before screen printing demonstrates the different quality of the ps Laser and ns Laser1 LCOs.

These results are in accordance to Fig. 2. Comparing the contact recombination velocity for low resistivity 1.5 Ωcm material in Fig. 3b with those values obtained on 200 Ωcm material in Fig. 3a, a significantly higher recombination velocity (around one order of magnitude) is found for the low resistivity material. The lowest contact recombination velocity of S_{cont} = 65 cm/s is observed for line contacts of width a = 250 µm processed with the ps Laser on 200 Ωcm material in Fig. 3a. In contrast, the contact reverse saturation current density $J_{0,cont}$ is lower on low resistivity material. Values of $J_{0,cont}$ as low as 900 fA/cm² are measured for line contacts on 1.5 Ωcm material in Fig. 3b. This value is comparable to those determined for a full area Al alloyed contact [14].

Furthermore, the contact recombination depends on the laser used for the LCOs. Lower contact recombination is feasible with contacts opened with the ps Laser, compared to ns Laser 1 and 2 in Fig. 3a) and b). To give an explanation for the observed difference in S_{cont}, we compare micrographs and SEM images of ps Laser and ns Laser 1 line contacts in Fig 4. The Al-doped BSF region appears brighter in the SEM image than the high resistivity bulk of the silicon wafer due to differing local ionization energies. We measure a mean back surface field (BSF) layer thickness of W_{BSF} = 1,4 µm at ns Laser 1 and W_{BSF} = 4,8 µm at the ps Laser. The mean BSF layer thickness W_{BSF} is determined by measuring the cross sectional area of the BSF and dividing it by the contact width. Due to smaller BSF layer thicknesses at the ns Laser 1 contacts, the contact recombination is increased [13].

The optical microscopic images in the upper left corner in Fig. 4a) and b) give an explanation for the reduced BSF thickness at the ns Laser contacts. We find low quality LCOs with no overlap at the ns Laser 1 line contact. Hence, the alloying process takes place independently at each single point contact. Remains of the dielectric layer probably prevent Si to dissolve in the Al melt between the single LCOs. Hence, the interface area between Si and Al is small with a high m_{Al}/A ratio. This leads to the formation of small BSF layers according to the argumentation of LBSF formation in reference 13 and the data in Fig. 3. Additionally cavities form, which are found to result in a thinner BSF. In contrast, at the ps Laser contact the alloying process takes place over the whole laser ablated area and a continuous BSF forms due to high quality and well overlapping LCOs.

In contrast to ps laser pulses, the relatively long ns laser pulses will affect the underlying silicon through heat dissipation in a depth of several µm [10] and defects are introduced in the Si bulk. However, while firing the sample, the Si dissolves into the Al melt. During cooling the liquid Si precipitates and grows defect free onto the Si substrate. A comparison of internal quantum efficiency (*IQE*) measurements of PERC cells comprising local Al alloyed contacts opened with UV ns laser and etching paste [3] demonstrated the general applicability of ns Lasers for local Al alloyed contacts.

5. Conclusion

We have presented measurements of the recombination at local Al alloyed contacts on high and low resistivity *p*-type FZ Si, employing an analytical model and calibration free lifetime measurements using the dynamic ILM technique. Laser contact openings (LCOs) through a locally opened dielectric stack are applied to the samples, before screen printing of an Al paste and firing.

The measured contact recombination velocity S_{cont} has been found to depend on the geometry and size of the contacts and the laser used for the LCOs. Extremely low surface recombination velocities of S_{cont} = 65 cm/s on high resistivity material and $J_{0,cont}$ = 900 fA/cm² at low resistivity material, demonstrate the significant improvement in contact recombination, employing local Al alloyed line contacts.

References

[1] Blakers A W,Wang A, Milne A M, Zhao J, Green M A. *22.8% efficient silicon solar cell*. 1989. Applied Physics Letters. Vol. 55. pp. 1363-1365. DOI: 10.1063/1.101596

[2] Gatz S, Hannebauer H, Hesse R, Werner F, Schmidt A, Dullweber T, Schmidt J, Bothe K, Brendel R. *19.4%-efficient large-area fully screen-printed silicon solar cells*. Phys. Status Solidi RRL 5, No. 4, 147–149 (2011) / DOI 10.1002/pssr.201105045

[3] Ramanathan S, Das A, Cooper I B, Rohatgi A, Payne A, Koehler I. *20% efficient screen printed LBSF cell fabricated using UV LASER for rear dielectric removal*. 2010. Proceedings of the 35th IEEE Photovoltaic Specialists Conference (IEEE, Hawaii, 2010). pp. 678-682

[4] Meemongkolkiat V, Nakayashiki K, Kim D S, Kim S, Shaikh A, Kuebelbeck A, Stockum W, Rohatgi A. *Investigation of modified screen-printing Al pastes for local back surface field formation*. 2006. Proceedings of the 32th IEEE Photovoltaic Specialists Conference (IEEE, Hawaii, 2006). pp. 1338-1341

[5] Uruena A, Hernandez J L, John J, Poortmans J, Mertens R. *Controlling the depth of the local Al BSF in PERC crystalline solar cells using alternative back side metallization.* 2010. Proceedings of the 25th European Photovoltaic Solar Energy Conference. (WIP, Valencia, 2010). pp. 2562-2564

[6] Uruena A, John J, Beaucarne G, Choulat P, Eyben P, Agostinelli G, Van Kerschaver E, Poortmans J, Mertens R. *Local Al-alloyed contacts for next generation Si solar cells.* 2009. Proceedings of the 24th European Photovoltaic Solar Energy Conference. (WIP, Hamburg, 2009). pp. 1483-1486

[7] Müller J, Bothe K, Gatz S, Haase F, Mader C and Brendel R. *Recombination at laser-processed local base contacts by dynamic infrared lifetime mapping.* 2010. Journal of Applied Physics. Vol. 108. 124513. DOI:10.1063/1.3517109

[8] Ramspeck K, Bothe K, Schmidt J and Brendel R. *Combined dynamic and steady-state infrared camera based carrier lifetime imaging of silicon wafers.* 2009. Journal of Applied Physics. Vol. 106. DOI: 10.1063/1.3261733

[9] Fischer B. *Loss Analysis of crystalline silicon solar cells using photoconductance and quantum efficiency measurements.* 2003. University Konstanz . PhD Thesis

[10] Engelhart P, Hermann S, Neubert T, Plagwitz H, Grischke R, Meyer R, Klug U, Schoonderbeek A, Stute U and Brendel R. *Laser ablation of SiO_2 for locally contacted Si solar cells with ultra-short pulses*. 2007. Progress in Photovoltaics, Vol. 15. pp. 521-527. DOI: 10.1002/pip.758

[11] Eidelloth S, Neubert T, Brendemuhl T, Hermann S, Giesel P, Brendel R. *High speed laser structuring of crystalline silicon solar cells.* 34th IEEE Photovoltaic Specialists Conference, 2009. p. 2389 - 2394 doi: 10.1109/PVSC.2009.5411310

[12] Plagwitz H, Schaper M, Schmidt J, Terheiden B, Brendel R. *Analytical model for the optimization of locally contacted solar cells.* 31st IEEE Photovoltaic Specialists Conference, 2005. p. 999-1002 doi: 10.1109/PVSC.2005.1488301

[13] Müller J, Bothe K, Gatz S , Plagwitz H , Schubert G and Brendel R. *Contact formation and recombination at screen-printed local Aluminum-alloyed Silicon solar cell base contacts*, Journal of Applied Physics, 2011, submitted

[14] Highly predictive modelling of entire Si solar cells for industrial applications. P.P. Altermatt, S. Steingrube, Y. Yang, C. Sprodowski, T. Dezhdar, S. Koc, B. Veith, S. Herrman, R. Bock, K. Bothe, J. Schmidt and R. Brendel. 2009. Proceedings of the 24th European Photovoltaic Solar Energy Conference. (WIP, Hamburg, 2009), pp. 901-906.